PHYSICAL REVIEW A **72**, 022507 (2005)

Interference effects in Auger resonant Raman spectra of CO via selective vibrational excitations across the O $1s \rightarrow 2\pi$ resonance

T. Tanaka,[1] H. Shindo,[1] C. Makochekanwa,[1,2] M. Kitajima,[1] H. Tanaka,[1] A. De Fanis,[3,4] Y. Tamenori,[3] K. Okada,[5] R. Feifel,[6,7] S. Sorensen,[8] E. Kukk,[4,9] and K. Ueda[4,*]

[1]*Department of Physics, Sophia University, Tokyo 102-8554, Japan*
[2]*Graduate School of Sciences, Kyushu University, Fukuoka 812-8581, Japan*
[3]*Japan Synchrotron Radiation Research Institute, Sayo-gun, Hyogo 679-5198, Japan*
[4]*Institute of Multidisciplinary Research for Advanced Materials, Tohoku University, Sendai 980-8577, Japan*
[5]*Department of Chemistry, Hiroshima University, Higashi-Hiroshima 739-8526, Japan*
[6]*Department of Physics, Uppsala University, Box 530, SE-751 21 Uppsala, Sweden*
[7]*Physical and Theoretical Chemistry Laboratory, Oxford University, South Parks Road, Oxford OX1 3QZ, United Kingdom*
[8]*Department of Synchrotron Radiation Research, Institute of Physics, University of Lund, Box 118, SE-221 00 Lund, Sweden*
[9]*Department of Physics, University of Turku, FIN-20014, Turku, Finland*

(Received 9 January 2005; published 18 August 2005)

The Auger resonant Raman spectra of CO, arising from the transitions to the *X* and *A* final electronic states of CO^+, have been recorded at photon energies corresponding to the vibrational excitations $v'=3,5$, and 8 in the O $1s \rightarrow 2\pi$ resonance. The spectra are simulated within the model that takes into account both the lifetime-vibrational interference (LVI) and interference with the nonresonant photoemission. The spectroscopic parameters, ω_e, $\omega_e x_e$, Γ and r_e, of the O $1s^{-1}2\pi$ core-excited state, necessary for the simulation, have been derived by fitting the Franck-Condon simulation to the total ion yield spectrum, assuming a Morse potential for the O $1s^{-1}2\pi$ state. Not only the LVI but also the interference with the nonresonant photoemission turn out to be significant.

DOI: 10.1103/PhysRevA.72.022507 PACS number(s): 33.60.Fy, 33.20.Rm

I. INTRODUCTION

Third generation, high-brilliance synchrotron radiation light sources offer high photon fluxes with very narrow photon bandwidths via high-resolution soft x-ray monochromators, and thus opportunities to investigate core excitation of molecules with photon bandwidths narrower than the lifetime widths [1–3]. Under this condition, the spectral width of the electron emission line via resonant excitation does not depend on the core-hole lifetime [4,5]; the so-called Auger resonant Raman condition. One of the interesting subjects that can be investigated under the Auger resonant Raman condition is the interference effect. Individual vibrational energy levels of the molecular core-excited state are broadened by the core-hole lifetime of the order of femtoseconds. If the lifetime width is of the same order as the vibrational spacing, then the vibrational levels overlap and thus the lifetime vibrational interference (LVI) [6–9] can be expected in the Auger resonant Raman spectrum [9–12]. The interference between the nonresonant and resonant photoemission [13–15] may also play a role in determining the vibrational distribution of the Auger resonant Raman spectrum [16,17].

The best-studied example of the resonant photoemission spectra seems to be the one for CO via the C $1s \rightarrow 2\pi$ resonance [10–12,16,17]. The lifetime width and vibrational spacing are about 0.1 eV and 0.3 eV, respectively, and thus the overlap is not significant. In spite of the small overlap, however, Osborne *et al.* [11] and Kukk *et al.* [12] clearly identified the influence of the LVI in the Auger resonant Raman spectra. Carravetta *et al.* [17], on the other hand, showed both experimentally and theoretically evidence for the interference effect between the nonresonant and resonant channels.

In the present paper, we report the first investigation of interference effects in the Auger resonant Raman spectra of CO via the O $1s \rightarrow 2\pi$ resonance. The O $1s \rightarrow 2\pi$ absorption (total ion-yield) spectrum of CO was studied by Püttner *et al.* [18] and Coreno *et al.* [19]. According to their investigation, the lifetime width and the vibrational spacing are about 0.15 eV and 0.17 eV, respectively, and thus the overlap of the vibrational components is larger than at the C $1s \rightarrow 2\pi$ resonance, and we can expect stronger LVI. Though the pioneering work on the resonant photoemission via the O $1s \rightarrow 2\pi$ resonance of CO was done by Piancastelli *et al.* [20], their resolution was insufficient to extract evidence for the LVI. Our simulation of the Auger resonant Raman spectra illustrates that both the LVI and the interference between resonant and nonresonant photoemission channels are important to reproduce the observed vibrational populations in the Auger resonant Raman spectra.

II. EXPERIMENT

The experiment was carried out at the high-resolution photochemistry beamline 27SU [21–23] at SPring-8 in Japan. The light source of this beamline is a figure-8 undulator [24]. The first-order harmonic light generated by this undulator has a horizontal linear polarization while the so-called 0.5th order harmonic light has a vertical polarization. The

*Email address: ueda@tagen.tohoku.ac.jp

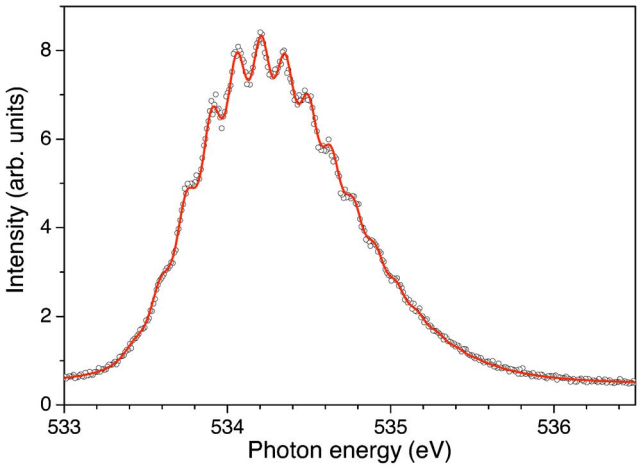

FIG. 1. (Color online) The O $1s \rightarrow 2\pi$ total ion yield spectrum of CO. The solid line represents the best fit to the experimental data points (open circles).

electron spectroscopy apparatus was described elsewhere [25] and only some specific features are summarized here. The apparatus consists of an electron energy analyzer (Gammadata-Scienta SES-2002), a gas cell, and a differentially pumped main chamber. The lens axis of the analyzer is set in a horizontal direction perpendicular to the photon beam. The whole system is on an adjustable stage so that the source point of the analyzer can be adjusted easily relative to the fixed beam position. For the angle resolved electron spectroscopy, the spectrometer is fixed in this state while switching the direction of the electric vector from horizontal to vertical, and vice versa. The degree of linear polarization was measured by observing the Ne $2s$ and $2p$ photolines. It was found to be larger than 0.98 for the current optical settings [26], thus enabling the assumption that all photons are completely polarized. Typical gas cell and analyzer pressures are $\sim 10^{-3}$ Torr and 10^{-7} Torr, respectively.

Before and after recording the electron spectra, ion yield spectra were recorded in a chamber upstream from the the electron spectrometer, where ions are collected by a dc field and detected by microchannel plates [27].

III. RESULTS AND DISCUSSION

A. The O $1s \rightarrow 2\pi$ ion yield spectrum

Figure 1 shows the measured total ion yield spectrum for the O $1s \rightarrow 2\pi$ resonance in CO. The spectrum clearly shows a vibrational progression, with the components significantly overlapped. Such overlap is mainly a consequence of the natural lifetime width being comparable to the vibrational spacing. As a natural consequence, strong LVI must be expected in the Auger resonant Raman spectra. This is in contrast with the well studied CO C $1s \rightarrow 2\pi$ excitation, where the three vibrational peaks $v'=0$, 1, and 2 are nearly separated, so that only a weak LVI was predicted and observed [8,11,12].

We extracted the spectroscopic parameters of the core-excited state from the total-ion yield spectrum in Fig. 1, assuming that the line shape of each vibrational component can be described with a Voigt profile and that the intensity distribution among these components is given by the Franck-Condon factors between the ground and core-excited states. We then performed a least-squares fitting [28] to the spectrum, taking as adjustable parameters the Gaussian width W (representing the photon bandwidth), the Lorentzian width Γ (representing the natural lifetime width), the level of a constant background and the energy and height of the first peak in the progression. The positions and heights of all other peaks in the progression are determined by the potential energy curves and nuclear wave functions of the ground and core-excited states. The accurately known literature values of the Morse parameters—vibrational frequency ω_e, anharmonicity $\omega_e x_e$, and equilibrium distance r_e—were used for the ground state [30] (see Table II), whereas for the core-excited state, ω_e, $\omega_e x_e$, and r_e were treated as free parameters. Thus the number of free parameters required to model the entire experimental spectrum in Fig. 1 is reduced to eight. The curve resulting from the fit is also depicted in Fig. 1 as the solid line through the data points. The photon bandwidth W thus determined was 48 meV. Other spectroscopic values extracted from the fit are summarized in Table I and compared with those from other measurements by Püttner *et al.* [18] and Coreno *et al.* [19]. The three measurements are in good agreement, confirming that the parameters describing the potential of the core-excited state are well established.

TABLE I. Spectroscopic constants of the O $1s^{-1}2\pi$ core-excited state, obtained via a least-squares fit to the total ion yield curve in Fig. 1 and those obtained by Püttner *et al.* [18] and Coreno *et al.* [19]: Γ, the lifetime width; ω_e, the vibrational frequency; $\omega_e x_e$, the anharmonicity; r_e the equilibrium distance.

	Present	Püttner [18]	Coreno [19]
Γ (meV)	156(10)	143(5)	158(8)
ω_e (meV)	167(1)	166(1)	166(3)
$\omega_e x_e$ (meV)	1.6(1)	1.8(1)	1.7(5)
r_e (Å)	1.288(1)	1.291(1)	1.292(1)

B. The Auger resonant Raman spectra

The ground state electronic configuration of the CO molecule is $(1\sigma)^2(2\sigma)^2(3\sigma)^2(4\sigma)^2(1\pi)^4(5\sigma)^2\ X\ ^1\Sigma^+$, where the 1σ corresponds to the O $1s$ core orbital. By a closer study of the x-ray emission intensities, Skytt *et al.* [31] concluded that the spectra reflect the local atomic $2p$ populations in the various valence orbitals around the core-hole sites. From their analysis, the outer valence orbitals 5σ, 1π, and 4σ have oxygen $2p$ character, and thus all these three orbitals can contribute to the Auger resonant Raman spectra via the participator Auger decay.

We recorded electron emission spectra at three energies across the O $1s \rightarrow 2\pi$ resonance; i.e., at 533.90 eV, 534.20 eV, and 534.62 eV, corresponding to the $v'=3$, 5, and 8 excitations, respectively. The photon and analyzer bandwidths were 59 meV and 31 meV, respectively, while the Doppler broadening was estimated to be 54 meV. Figure

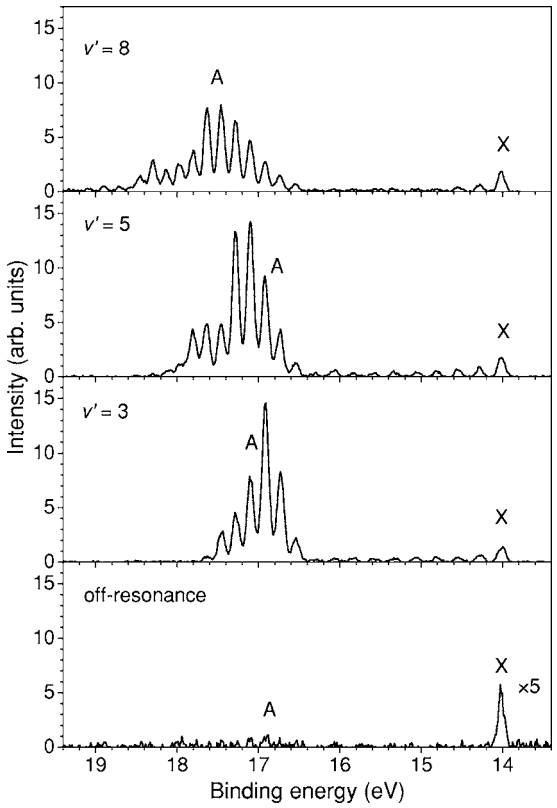

FIG. 2. Measured electron emission spectra from the two outermost valence orbitals at three different excitation energies corresponding to excitations to the $v'=3$, 5, and 8 vibrational components of the O $1s^{-1}2\pi$ core-excited state (resonant spectra) and at an energy of 530.92 eV, i.e., below the resonance ("nonresonant" spectrum).

2 shows the resulting electron spectra. Each spectrum shows the two bands corresponding to the transitions to the X $5\sigma^{-1}\,{}^2\Sigma^+$ and A $1\pi^{-1}\,{}^2\Pi$ electronic final states in the binding energy range 13.4–19.4 eV.

For comparison, the spectrum recorded at 530.92 eV (hereafter referred to as the "nonresonant" spectrum), which is below the resonant excitation energies, is also included. One may notice that the intensity of the A band relative to the the X band is significantly weak in the present spectrum at 530.92 eV, in comparison with the photoelectron spectrum recorded with the helium lamp (see, for example [29]). This is partly due to the destructive interference between the resonant and nonresonant photoionization channels and will be discussed later. Compared to the spectrum at 530.92 eV, the resonant spectra show resonance enhancement and altered vibrational populations for the two bands. The vibrational progression of the A state exhibits a characteristic distribution that varies significantly as the vibrational quantum number v' of the intermediate core-excited states increases from 3 to 8. With the increase in v', higher vibrational components appear and form the second peak in the vibrational distribution at $v''=6$ for $v'=5$ and at $v''=10$ for $v'=8$. The vibrational distribution in the X band, on the other hand, also show resonant enhancement but their dependence on the vibrational quantum number v' of the core-excited state is not as significant as the A band. The X band, which consists of only one peak ($v''=0$) in the spectrum at 530.92 eV, extends over a wide energy range and overlaps the A band.

TABLE II. Spectroscopic constants for the initial and final states of the Auger resonant Raman process [30]. See Table I for explanation of the symbols.

	CO	CO^+	
	ground state	$(X\,{}^2\Sigma^+)$	$(A\,{}^2\Pi)$
ω_e (meV)	269.020	274.53	193.67
$\omega_e x_e$ (meV)	1.648	1.880	1.678
r_e (Å)	1.1283	1.115	1.244

C. Lifetime vibrational interference (LVI) effects

LVI is well documented in the literature [6–12] and thus we present here only the final expression for the intensity of the vibrational component f of the final ionic state at the excitation energy ω as

$$I_f^{LVI}(\omega) = |M|^2 \left| \sum_n \frac{\langle f|n\rangle\langle n|0\rangle}{\omega - \omega_{n0} + i\frac{\Gamma}{2}} \right|^2, \qquad (1)$$

where $|M|$ is the electronic transition moment for the Auger resonant Raman process concerned, $|0\rangle$, $|n\rangle$, $|f\rangle$ denote vibrational wavefunctions of the initial ground state, intermediate core-excited state, and final ionic state, respectively. Γ is the lifetime width of the core-excited state, and ω_{n0} is the energy of the core-excited vibrational state $|n\rangle$ relative to the ground vibrational state $|0\rangle$.

We have simulated the Auger resonant Raman spectra using Eq. (1) for each of the two bands X and A. The vibrational wavefunctions $|0\rangle$ and $|f\rangle$ for the initial ground state and the final ionic state of the Auger resonant Raman process are calculated using the spectroscopic constants of these states given in Ref. [30] and summarized in Table II, while the vibrational wave functions $|n\rangle$ for the intermediate core-excited state are calculated using the constants obtained as explained above and presented in Table I. In the simulation, there is only one fitting parameter $|M|^2$ for each band. This parameter is a scaling factor for the total intensity of the band and may be expected to be independent of the excitation energy. The variations in the band's total intensity with the excitation energy are then entirely determined by the sum in Eq. (1). In the practical fitting to the integrated intensity for each band, however, $|M|^2$ is treated as a fitting parameter for each different excitation energy.

The simulated spectra are compared with the experimental spectra in the upper panels of Figs. 3–5, where the excitation energies correspond to $v'=3$, 5, and 8, respectively. In Eq. (1), we neglected the contribution from the nonresonant channel. Thus, for the comparison, we subtracted the experimental "nonresonant" spectrum (the bottom panel in Fig. 2) from the experimental resonant spectra (the upper three spectra in Fig. 2). As can be seen in the figure, there is good qualitative agreement between the simulated and measured individual spectra of all three different excitations.

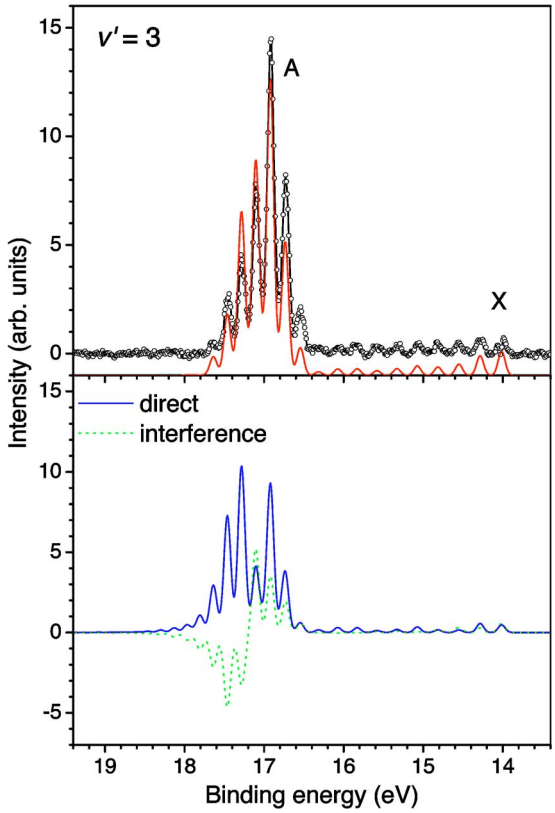

FIG. 3. (Color online) Upper panel: The measured (circles) and simulated (solid line) electron emission spectra via excitation to $v'=3$ of the O $1s^{-1}2\pi$ core-excited state. The simulation includes only the LVI. The presented experimental spectra are the difference between the resonant and "nonresonant" spectra. See text for the details. Lower panel: direct (solid blue line) and interference (dotted green line) terms defined by Eq. (2).

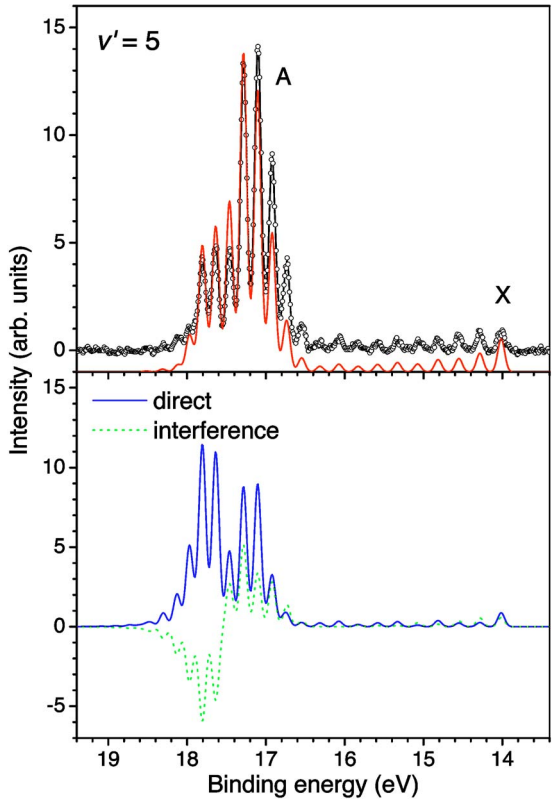

FIG. 4. (Color online) The measured (circles) and simulated (solid line) electron emission spectra via excitation to $v'=5$ of the O $1s^{-1}2\pi$ core-excited state. See the caption of Fig. 3 and text for the details.

To investigate the LVI explicitly, we rewrite Eq. (1) as

$$I_f^{LVI}(\omega) = |M|^2 \sum_n \left| \frac{\langle f|n\rangle\langle n|0\rangle}{\omega - \omega_{n0} + i\frac{\Gamma}{2}} \right|^2 + |M|^2 \sum_{m\neq n} \frac{\langle f|n\rangle\langle n|0\rangle}{\omega - \omega_{n0} + i\frac{\Gamma}{2}} \frac{\langle f|m\rangle\langle m|0\rangle}{\omega - \omega_{m0} - i\frac{\Gamma}{2}}, \quad (2)$$

where the first and second terms on the right-hand side are called the direct term and the interference term, respectively. The lower panels of Figs. 3–5 display the contributions from the direct and interference terms separately. As can be seen in the figures, the interference term is as significant as the direct term and plays a role in redistributing the vibrational population. By a closer look at the most prominent *A* band, one can clearly see that the LVI enhances the population of the lower vibrational components and suppresses the population of the higher vibrational components.

D. Interference effect between the resonant and nonresonant channels

The inclusion of the nonresonant channel is straightforward [15,17]. In analog to Eq. (1), we have

$$I_f(\omega) = \left| D\langle f|0\rangle + M\sum_n \frac{\langle f|n\rangle\langle n|0\rangle}{\omega - \omega_{n0} + i\frac{\Gamma}{2}} \right|^2, \quad (3)$$

where the term $D\langle f|0\rangle$ stands for the direct photoionization to the final ionic state. In Eq. (3), the parameters to be determined are two, M and D, or alternatively a ratio $|D/M|^2$ and an intensity scaling factor $|D|^2$. These parameters for each band were determined so that the "nonresonant" and resonant experimental spectra were well reproduced by the simulated spectra. Positive values were chosen for both M and D for both bands since choosing the negative value for one of them worsened the agreement with the experiment significantly. It should be noted that the experimental "nonresonant" spectrum is not necessarily recorded far away from the resonance where the resonant contribution disappears. As pointed out in the previous subsection, the spectrum recorded at 530.92 eV is affected by the interference between the resonant and nonresonant channels. However, since this interference effect is taken into account by Eq. (3), we can still use the spectrum at 530.92 eV together with the resonant spectrum, in order to extract $|D/M|^2$. To confirm our algorithm and to check the sensitivity of the choice of the nonresonant spectrum, we used also the nonresonant spectrum recorded at 528.60 eV at lower resolution and determined the ratio $|D/M|^2$. The results are almost the same.

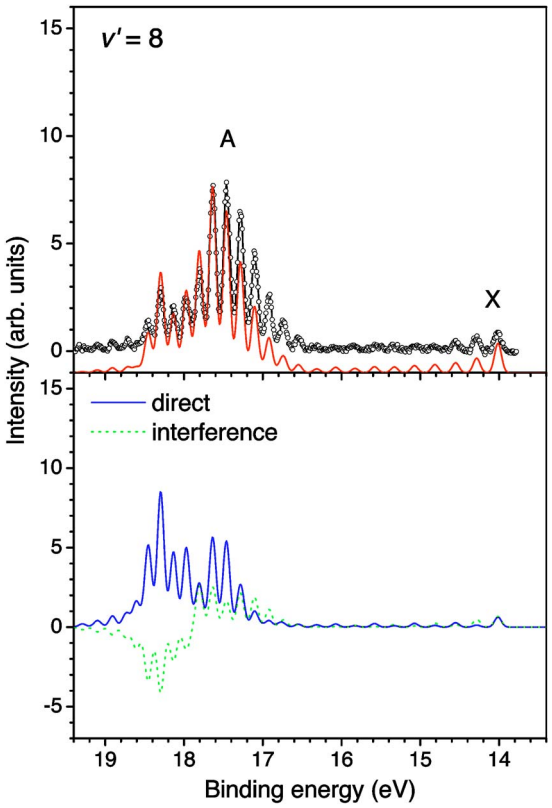

FIG. 5. (Color online) The measured (circles) and simulated (solid line) electron emission spectra via excitation to $v'=8$ of the O $1s^{-1}2\pi$ core-excited state. See the caption of Fig. 3 and text for the details.

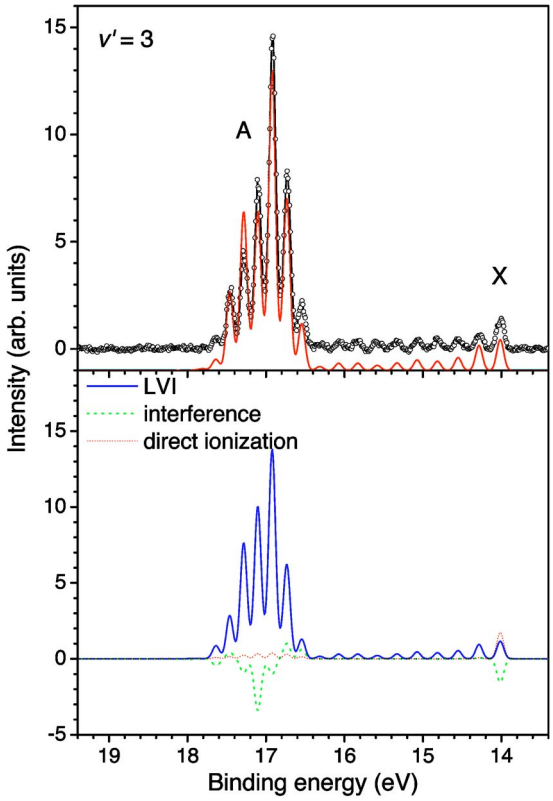

FIG. 6. (Color online) Upper panel: The measured (circles) and simulated (solid red line) spectra via excitation to $v'=3$ of the O $1s^{-1}2\pi$ core-excited state. The simulation includes both the LVI and the interference with the direct photoionization channel. The experimental spectrum is the same as the resonant spectrum in Fig. 2. See text for the details. Lower panel: LVI (solid blue line), direct photoionization (thin dotted red line) and interference (dotted green line) terms defined by Eq. (4).

In the upper panels of Figs. 6–8, the spectra simulated by using Eq. (3) are compared with the experimental spectra. Here the experimental spectra are identical to those in Fig. 2, i.e., no subtraction of the "nonresonant" contribution was made. Comparing the upper panels of Figs. 3–5 and Figs. 6–8, one can see that the agreement between the simulated and measured spectra is improved by taking the contribution from the nonresonant channel into account. The improvement is most apparent for the lower vibrational components of the A band.

To investigate the interference between the resonant and nonresonant channels explicitly, we rewrite Eq. (3) as

$$I_f(\omega) = I_f^{LVI}(\omega) + |D\langle f|0\rangle|^2 + \sum_n \frac{2DM(\omega-\omega_{n0})\langle f|0\rangle\langle f|n\rangle\langle n|0\rangle}{(\omega-\omega_{n0})^2+\frac{\Gamma^2}{4}}, \quad (4)$$

where the first term is given by Eq. (1) and represents the LVI-modified resonant emission. The second term represents the nonresonant portion of the emission intensity and the third term represents the interference between the resonant and nonresonant channels.

In the lower panels of Figs. 6–8, we plot these three contributions separately. Let us focus on the A band. Though the nonresonant intensity $|D\langle f|0\rangle|^2$ is indeed negligible in comparison with the resonant contribution $I_f^{LVI}(\omega)$, the interference term [the third term of Eq. (4)] significantly contributes to the total intensity $I_f(\omega)$. We compare the contribution from each of these channels to the A band intensity, examining the spectra shown in the lower panel of Figs. 3–5 and Figs. 6–8. In the simulations in Figs. 3–5, only the LVI effect was considered. This resulted in enhancement and suppression of the populations of the lower and higher vibrational components, respectively, and in consequence, the simulated spectra were significantly different from the measured ones. As clearly shown by the spectrum labeled "interference" in the bottom panels of Figs. 6–8, the contribution from interference between the resonant and nonresonant channels enhances the populations for the low vibrational components and suppresses the populations for the intermediate vibrational components. Due to the enhancement and suppression for the low and intermediate vibrational components, respectively, the agreement between the experimental and simulated spectra is greatly improved.

Finally, we comment briefly on the energy dependence of $|M|^2$. In the simulation, this parameter was not fixed for different excitation energies. The energy dependence, if there is, may be attributed to the dependence of the Auger transition amplitude on the internuclear distance, neglected in Eq. (3)

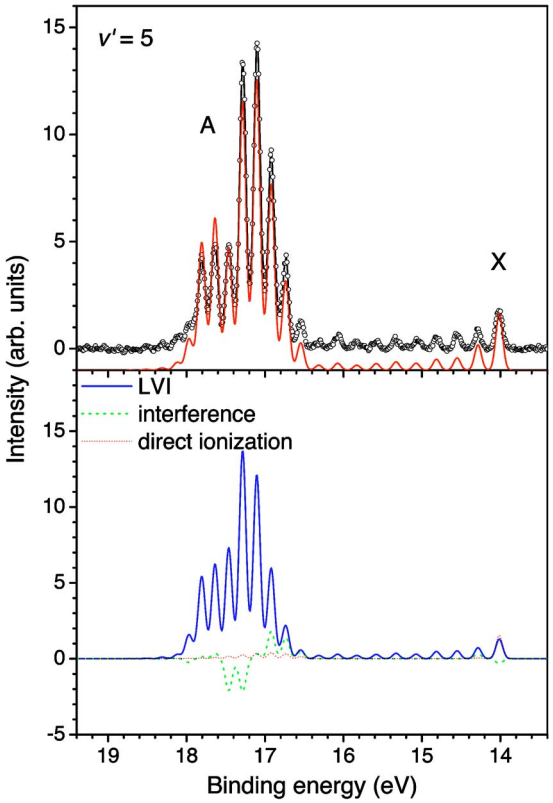

FIG. 7. (Color online) The measured (circles) and simulated (solid red line) spectra via excitation to $v'=5$ of the O $1s^{-1}2\pi$ core-excited state. See the caption of Fig. 6 and text for the details.

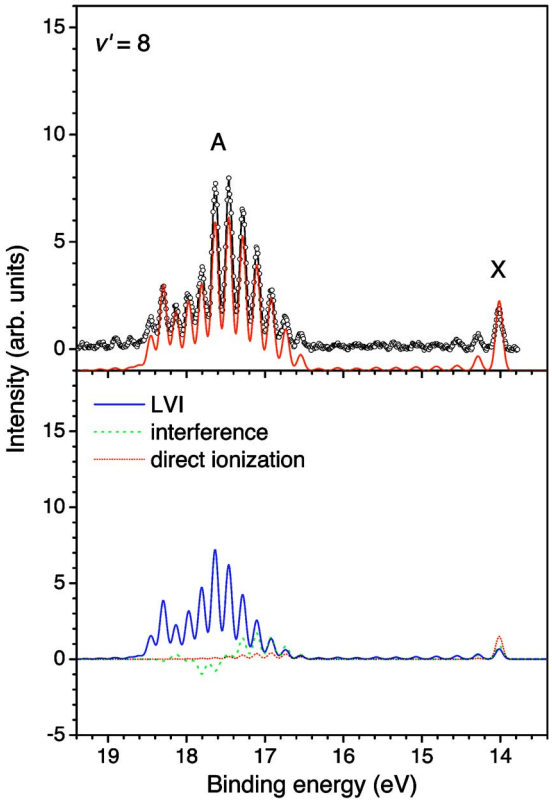

FIG. 8. (Color online) The measured (circles) and simulated (solid red line) spectra via excitation to $v'=8$ of the O $1s^{-1}2\pi$ core-excited state. See the caption of Fig. 6 and text for the details.

[32]. The ratio of $|M|^2$ resulting from the excitations to $v'=3$, 5, and 8 is 101:100:80 for the X band and 91:100:112 for the A band. These ratios may suggest the existence of the energy dependence of $|M|^2$. The change is, however, of the order of the experimental uncertainty ($\sim 10\%$). We cannot draw a decisive conclusion about the energy dependence of the Auger amplitudes from the present experiment.

IV. CONCLUSION

We have measured the Auger resonant Raman spectra of CO, arising from the transitions to the $X\ 5\sigma^{-1}\ ^2\Sigma^+$ and $A\ 1\pi^{-1}\ ^2\Pi$ final cationic states of CO^+, at photon energies corresponding to the excitations to the vibrational components $v'=3$, 5, and 8 in the O $1s\rightarrow 2\pi$ resonance. To elucidate on the various interference effects in the electron emission process, we have performed various simulations. The spectroscopic parameters, ω_e, $\omega_e x_e$, and r_e, of the O $1s^{-1}2\pi$ core-excited state, necessary for the simulation, have been derived by fitting the Franck-Condon simulation to the total ion yield spectrum, assuming a Morse potential for the O $1s^{-1}2\pi$ state. The simulation of the electron emission spectra that takes into account only the LVI reproduces the measured spectra semiquantitatively. The simulation that takes into account both the LVI and the interference between the resonant and nonresonant channels results in better agreement with experimental spectra. The contribution from the interference term between the resonant and nonresonant channels turns out to be significant. The experimental results may imply the existence of the dependence of the Auger amplitudes on the internuclear distance. However, we cannot draw a decisive conclusion. We hope that *ab initio* theoretical calculations will confirm it.

ACKNOWLEDGMENTS

This work was carried out with the approval of the SPring-8 program review committee (proposal No. 2001B0082-NS-np) and partly supported by the Grants-in-Aid for Scientific Researches from the Japan Society for Promotion of Science (JSPS). The authors are grateful to the staff of SPring-8 for their help during the experiments. C.M. is also grateful to the JSPS for financial support under Grant No. P04064. E.K. is grateful to Tohoku University for hospitality and financial support during his stay there.

[1] S. L. Sorensen and S. Svensson, J. Electron Spectrosc. Relat. Phenom. **114–116**, 1 (2001).
[2] K. Ueda, J. Phys. B **36**, R1 (2003).
[3] J. D. Bozek, S. E. Canton, E. Kukk, and N. Berrah, Chem. Phys. **289**, 149 (2003).
[4] T. Åberg and B. Crasemann, in *Resonant Anomalous X-Ray Scattering*, edited by G. Materlik, C. J. Sparks, and K. Fisher (North-Holland, Amsterdam, 1994).
[5] A. Kivimäki, A. Naves de Brito, S. Aksela, H. Aksela, O.-P. Sairanen, A. Ausmees, S. J. Osborne, L. B. Dantas, and S. Svensson, Phys. Rev. Lett. **71**, 4307 (1993).
[6] F. Kh. Gel'mukhanov, L. N. Mazalov, and A. V. Kondratenko, Chem. Phys. Lett. **46**, 133 (1977).
[7] F. Kaspar, W. Domcke, and L. S. Cederbaum, Chem. Phys. **44**, 33 (1979).
[8] P. Skytt, P. Glans, K. Gunnelin, J. Guo, and J. Nordgren, Phys. Rev. A **55**, 146 (1997).
[9] J.-E. Rubensson, M. Neeb, M. Biermann, and W. Eberhardt, J. Chem. Phys. **99**, 1633 (1993).
[10] M. Neeb, J.-E. Rubensson, M. Biermann, and E. Eberhardt, J. Electron Spectrosc. Relat. Phenom. **67**, 261 (1994).
[11] S. J. Osborne, A. Ausmees, S. Svensson, A. Kivimäki, O.-P. Sairanen, A. Naves de Brito, H. Aksela, and S. Aksela, J. Chem. Phys. **102**, 7317 (1995).
[12] E. Kukk, J. D. Bozek, W.-T. Cheng, R. F. Fink, A. A. Wills, and N. Berrah, J. Chem. Phys. **111**, 9642 (1999).
[13] U. Fano, Phys. Rev. **124**, 1866 (1961).
[14] R. Camilloni, M. Zitnik, C. Comicioli, K. C. Prince, M. Zacchigna, C. Crotti, C. Ottaviani, C. Quaresima, P. Perfetti, and G. Stefani, Phys. Rev. Lett. **77**, 2646 (1996).
[15] A. De Fanis, N. Saito, H. Yoshida, Y. Senba, Y. Tamenori, H. Ohashi, H. Tanaka, and K. Ueda, Phys. Rev. Lett. **89**, 243001 (2002).
[16] M. N. Piancastelli, M. Neeb, A. Kivimäki, B. Kempgens, H. M. Köppe, K. Maier, and A. M. Bradshaw, Phys. Rev. Lett. **77**, 4302 (1996).
[17] V. Carravetta, F. Kh. Gel'mukhanov, H. Ågren, S. Sundin, S. J. Osborne, A. Naves de Brito, O. Björneholm, A. Ausmees, and S. Svensson, Phys. Rev. A **56**, 4665 (1997).
[18] R. Püttner, I. Dominguez, T. J. Morgan, C. Cisneros, R. F. Fink, E. Rotenberg, T. Warwick, M. Domke, G. Kaindl, and A. S. Schlachter, Phys. Rev. A **59**, 3415 (1999).
[19] M. Coreno, M. de Simone, K. C. Prince, R. Richter, M. Vondracek, L. Avaldi, and R. Camilloni, Chem. Phys. Lett. **306**, 269 (1999).
[20] M. N. Piancastelli, M. Neeb, A. Kivimäki, B. Kempgens, H. M. Köppe, K. Maier, A. M. Bradshaw, and R. F. Fink, J. Phys. B **30**, 5677 (1997).
[21] H. Ohashi, E. Ishiguro, Y. Tamenori, H. Kishimoto, M. Tanaka, M. Irie, T. Tanaka, and T. Ishikawa, Nucl. Instrum. Methods Phys. Res. A **467–468**, 529 (2001).
[22] H. Ohashi, E. Ishiguro, Y. Tamenori, H. Okumura, A. Hiraya, H. Yoshida, Y. Senba, K. Okada, N. Saito, I. H. Suzuki, K. Ueda, T. Ibuki, S. Nagaoka, I. Koyano, and T. Ishikawa, Nucl. Instrum. Methods Phys. Res. A **467–468**, 533 (2001).
[23] Y. Tamenori, H. Ohashi, E. Ishiguro, and T. Ishikawa, Rev. Sci. Instrum. **73**, 1588 (2002).
[24] T. Tanaka and H. Kitamura, J. Synchrotron Radiat. **3**, 47 (1996).
[25] Y. Shimizu, K. Nagao, K. Ueda, M. Takahashi, H. Chiba, S. Yanagida, M. Okunishi, K. Ohmori, Y. Sato, T. Hayaishi, and K. J. Ross, J. Electron Spectrosc. Relat. Phenom. **88–91**, 1031 (1998).
[26] H. Yoshida, Y. Senba, M. Morita, T. Goya, A. De Fanis, N. Saito, K. Ueda, Y. Tamenori, and H. Ohashi, in *Synchrotron Radiation Instrumentation: 8th International Conference on Synchrotron Radiation Instrumentation*, edited by T. Warwick, J. Arthur, H. A. Padmore, and J. Stöhr, AIP Conf. Proc. No. 705 (AIP, Melville, NY, 2004), p. 267.
[27] N. Saito, K. Ueda, M. Simon, K. Okada, Y. Shimizu, H. Chiba, Y. Senba, H. Okumura, H. Ohashi, Y. Tamenori, S. Nagaoka, A. Hiraya, H. Yoshida, E. Ishiguro, T. Ibuki, I. H. Suzuki, and I. Koyano, Phys. Rev. A **62**, 042503 (2000).
[28] For curve fitting the program SPANCF was used. URL: http://www.geocities.com/ekukk
[29] D. W. Turner, C. Baker, A. D. Baker, and C. R. Brundle, *Molecular Photoelectron Spectroscopy* (Wiley, London, 1970).
[30] K. P. Huber and G. Herzberg, *Molecular Spectra and Molecular Structure IV* (Van Nostrand Reinhold, New York, 1979).
[31] P. Skytt, P. Glans, K. Gunnelin, J. Guo, J. Nordgren, Y. Luo and H. Ågren, Phys. Rev. A **55**, 134 (1997).
[32] M. N. Piancastelli *et al.*, J. Phys. B **33**, 1819 (2000).